Fall 12-2019

Sparse Transducer Imaging

Sen Bing
Southern Methodist University, sbing@smu.edu

SPARSE TRANSDUCER IMAGING

Approved by:

Carlos E. Davila
Associate Professor of Electrical and
Computer Engineering

J.-C. Chiao
Professor of Electrical and Computer
Engineering

Dinesh Rajan
Professor of Electrical and Computer
Engineering

SPARSE TRANSDUCER IMAGING

A Master Thesis Presented to the Graduate Faculty of the

Lyle School of Engineering

Southern Methodist University

in

Partial Fulfillment of the Requirements

for the degree of

Master of Science in Electrical Engineering

with a

Major in Electrical Engineering

by

Sen Bing

B.S., Electrical Engineering, Hainan Normal University

December 21, 2019

ACKNOWLEDGMENTS

I would like to express my sincere gratitude to Prof. Davila for his wise guidance, patience, and continuous help.

Bing, Sen B.S., Electrical Engineering, Hainan Normal University

SPARSE TRANSDUCER IMAGING

Advisor: Carlos E. Davila

Master of Science in Electrical Engineering degree conferred Dec 21,2019
Master Thesis completed Dec 5,2019

Ultrasound is commonly used in medicine for imaging different organ systems. Also, it is widely used to monitor fetal development. The most common ultrasound imaging technique is B-mode, which uses an array of transducers to generate a narrow beam.

The array with dynamic focusing is implemented by phase shifters which are complex and costly. Also, the beamwidth is not sufficiently narrow which means it can not provide high resolution. My research will investigate a new method which doesn't need narrow beam and can be implemented by only one transducer. The new system can give potentially higher resolution and significantly reduce the cost compared to conventional B-mode ultrasound imagers.

TABLE OF CONTENTS

LIST OF FIGURES

To my grandpa, who I deeply love but didn't catch the last sight.

CHAPTER 1
INTRODUCTION

1.1. Motivation

Today, ultrasound imaging is widely used to monitor fetal development and detect disease of the kidney, liver, and heart since it is safe and relatively low cost [4]. The most common ultrasound imaging technique is Brightness Mode (B-Mode), this system uses an array of transducers to generate a narrow beam which is scanned along a slice of tissue through delay and sum beamforming [3]. The back-scattered energy from the scanned beam can be used to reconstruct the tissue slice and therefore a 2-D image of the human body can be generated.

But there are some shortcomings in B-mode ultrasound imaging. The first is that the array with dynamic focusing is implemented by phase shifters which are complex and costly. The second is that array aperture is limited so that the beamwidth is not sufficiently narrow which means it can not provide high resolution. So the ultrasound images tend to be blurred [9].

This research will demonstrate a new method of generating the ultrasound image which doesn't need phase shifting. The new method will only use one or two transducers with higher resolution and lower cost compared to the B-mode ultrasound image systems. We call the method Sparse Transducer Imaging (STI).

1.2. Overview of Ultrasound Imaging Systems

The neurologist Karl Dussuk is credited with being the first to use ultrasonic waves as a diagnostic tool in 1942. Ultrasound technology and its application in medical care have become more mature. There are many types of ultrasound imaging systems but the main idea is the same. After transmitting the ultrasound signal, the system can determine the corresponding location of a scatterer by the arrival time of the received signal since the tissue boundaries cause reflections. Ultrasound imaging can be classified into different categories depending on their operation and purpose. This section gives an overview of common ultrasound imaging methodologies.

1.2.1. A-Mode

A-mode (Amplitude-mode) imaging is a one-dimensional method which records the pulse echo field along a single line [1]. It is often used to judge the depth of an organ and early pregnancy assessment like detection of fetal heart beat or placental localization, as well as for sinusitis diagnosis [5]. A simple A-mode system is shown in Figure 1.1.

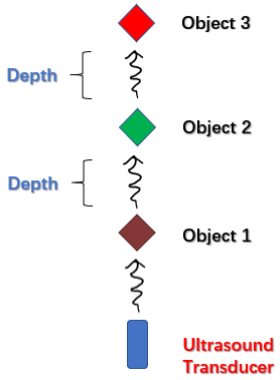

Figure 1.1. An A-mode ultrasound imaging system.

The transducer transmits the pulse and the receiver (same transducer) senses three sets of reflections since there are three objects on one line. The system can be simulated in MATLAB and the received signal is shown in Figure 2. There are three clusters in Figure 2 but separated in time, which indicates the depth between the three objects. Each cluster represents one object in the A-mode system and the interval of time is for the transmitted pulse to get the object from and reflect back to the receiver.

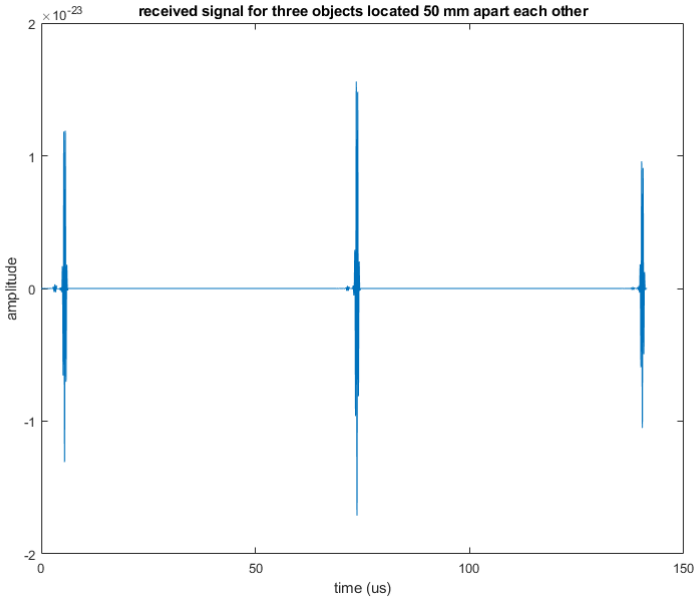

Figure 1.2. Received echo pulse with three objects located equally apart in A-mode system.

1.2.2. B-Mode

B-Mode (Brightness-mode) is the most common ultrasound imaging method which can implement the 2-D cross-sectional image representing tissues and organ boundaries within the body [2]. Like A-mode, it is constructed from echoes which are generated by reflection of transmitted ultrasound waves on tissue boundaries and some small irregularities inside

the tissues. It can be viewed as repeated A-mode scans to generate the 2-D image. Each echo is shown at a pixel (point) in the image corresponding to the relative position of its origin within the body cross section. The brightness of 2-D image on each point is related to the amplitude of the echo so that these different brightness points can form the 2-D scaled map which shows the scanning result of tissues or organ boundaries.

Like we described above, the 2-D B-mode image is formed by a great number of A-mode lines which are produced by pulse-echo sequence. In each line, the space closer to the transducer, the faster the echoes return from the targets. Therefore, the depth below the transducer determines the gray scale of the image. A complete B-mode image is made up about 100 or more A-mode lines. Let's take the linear array transducer for example, as shown in Figure 1.3 a. Also, there is a B-mode ultrasound image which included a human fetus, as shown in Fig.1.3 b.

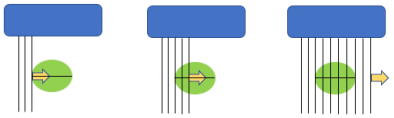

(a)

(b)

Figure 1.3. B-mode. (a) Formation of a 2-D B-mode image. (b) B-mode ultrasound image.

An image line is formed during the first pulse-echo sequence and the active area of the transducer is then stepped along the array to the adjacent beam position until there is a new image line at each position and generate the 2-D image by using these image lines. Fig 1.3a shows a linear scan. Alternately, the beam can be scanned along an arc using phase shifters and delay-sum beamforming [3].

1.2.3. M-Mode

M-Mode (Motion Mode) also called TM-Mode (Time Motion Mode) is a type of one-dimensional image to analyze moving body parts [6]. An a example of M-mode, as shown in Fig 1.4 [3].

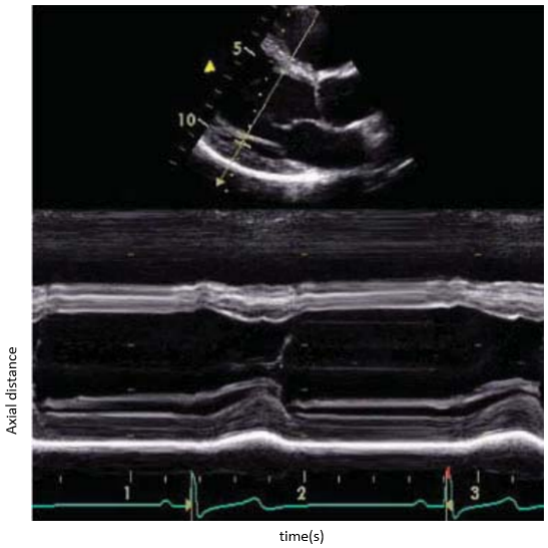

Figure 1.4. M-mode image.

In Fig 1.4, the M-mode image is shown below a B-mode image. The user can select a particular scan line in the B-mode image, which is displayed over time as the M-mode scan. An M-mode trace takes A-mode echos from a single direction and traces out the

movement of targets with time. The stationary part of a target like the chest wall forms horizontal lines and the moving part of a target like the heart values will be recorded over time. M-mode is commonly used in cardiac and fetal cardiac imaging.

CHAPTER 2
OVERVIEW OF ULTRASOUND FIELD PHYSICS

In this chapter, we will focus on the basic physics of ultrasound wave propagation and the calculation of the scattered or incident field. It will give us the theoretical basis for ultrasound wave propagation and a better understanding of ultrasound's underlying physics. This chapter is based on Jensen's paper named "A model for the propagation and scattering of ultrasound in tissue" [7].

2.1. Ultrasound Wave Propagation

Ultrasound propagates by changing the pressure in a medium. In this section, we will derive the wave equation needed to present an overview of ultrasound wave propagation. To do that, we need to make two assumptions [7]. The first assumes that instantaneous acoustic pressure and density can be written as

$$P_{ins}(r,t) = P + p_1(r,t), \tag{2.1}$$

$$\rho_{ins}(r,t) = \rho(r) + \rho_1(r,t), \tag{2.2}$$

Where P is the mean pressure of the medium and ρ is is the density of the undisturbed medium. Both the pressure change p_1 and the density change ρ_1 are caused by the ultrasound wave and they are small compared to P and ρ.

The second assumption is there is no heat conduction or conversion of ultrasound to thermal energy. So the acoustic pressure P_{ins} and densityρ_{ins} satisfy the adiabatic equation.

$$\frac{dP_{ins}}{dt} = c^2 \frac{d\rho_{ins}}{dt} \tag{2.3}$$

In the Euler description, the equation above can be written as

$$\frac{1}{c^2}\frac{\partial p_1}{\partial t} = \frac{\partial \rho_1}{\partial t} + u \cdot \Delta\rho \tag{2.4}$$

where u is the particle velocity, ∇ is the gradient operator and $\cdot$ is the dot product.

Meanwhile, the pressure, density and particle velocity also satisfy the hydrodynamics equations:

$$\rho_{\text{ins}}\,\frac{d\mathbf{u}}{dt} = -\nabla P_{\text{ins}} \tag{2.5}$$

$$\frac{\partial \rho_{\text{ins}}}{\partial t} = -\nabla \cdot (\rho_{\text{ins}}\,\mathbf{u}) \tag{2.6}$$

Assume that propagation velocity and the density only vary slightly from their mean values, we can get:

$$\begin{aligned} \rho(\mathbf{r}) &= \rho_0 + \Delta\rho(\mathbf{r}) \\ c(\mathbf{r}) &= c_0 + \Delta c(\mathbf{r}) \end{aligned} \tag{2.7}$$

where $\rho_0 \gg \Delta\rho$ and $c_0 \gg \Delta c$. With the equations above, we can get the wave equation [7]:

$$\nabla^2 p_1 - \frac{1}{c_0^2}\frac{\partial^2 p_1}{\partial t^2} = -\frac{2\Delta c}{c_0^3}\frac{\partial^2 p_1}{\partial t^2} + \frac{1}{\rho_0}\mathbf{v}(\Delta\rho)\cdot\mathbf{v}_{p_1} \tag{2.8}$$

where the two terms on the right side are scattering terms which vanish for a homogeneous medium.

2.2. Calculation of The Incident Field

In this section, we will calculate the incident field generated by the ultrasound transducer. There are many ways to calculate the incident field but we will introduce the convolution method developed by Tupholme and Stepanishen which is used by Jensen to develop the FIELD II platform [8]. We use FIELD II as our main tool to implement our simulations.

The incident field can be calculated by solving the wave equation for the homogeneous case:

$$\nabla^2 p_1 - \frac{1}{c_0^2}\frac{\partial^2 p_1}{\partial^2 t} = 0 \tag{2.9}$$

For convenience, we apply the velocity potential $\psi(\mathbf{r}, t)$ which also satisfies the wave equation for a homogeneous medium:

$$\nabla^2 \psi - \frac{1}{c_0^2}\frac{\partial^2 \psi}{\partial^2 t} = 0 \tag{2.10}$$

the pressure can be found as:

$$p(\mathbf{r}, t) = \rho_0 \frac{\partial \psi(\mathbf{r}, t)}{\partial t} \tag{2.11}$$

Next, we use the coordinate system in figure 2.1 where the particle velocity normal to the transducer surface is denoted by $v\left(\mathbf{r}_3 + \mathbf{r}_4, t\right)$.

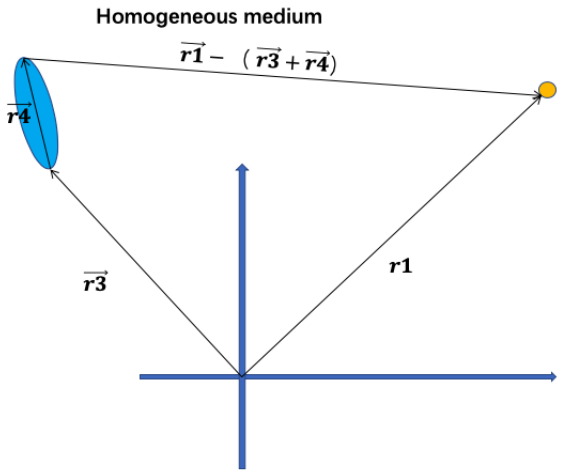

Figure 2.1. Coordinate system for calculating the incident field.

If the aperture is set up as an infinite, rigid, and flat baffle, the solution to the homogeneous wave equation is

$$\psi\left(\mathbf{r}_1 + \mathbf{r}_3, t\right) = \int_s \int_T v\left(\mathbf{r}_3 + \mathbf{r}_4, t_3\right) g\left(\mathbf{r}_1, t | \mathbf{r}_3 + \mathbf{r}_4, t_3\right) dt_3 d^2\mathbf{r}_4 \tag{2.12}$$

where S denotes the transducer surface, and g is the Green's function for a bounded medium, given by

$$g\left(\mathbf{r}_1, t|\mathbf{r}_3+\mathbf{r}_4, t_3\right) = \delta\left(t-t_3-\left|\mathbf{r}_1-\mathbf{r}_3-\mathbf{r}_4\right|/c_0\right)/\left(2\pi\left|\mathbf{r}_1-\mathbf{r}_3-\mathbf{r}_4\right|\right) \tag{2.13}$$

where c_0 is the mean propagation velocity and $|\mathbf{r}_1-\mathbf{r}_3-\mathbf{r}_4|$ is the distance from the transducer S to the field point we set. The integral is a statement of Huyghens'principle that the resulting field is made up by integrating the contributions from a spherical wave generated by each point on the transducer [7].

If the particle velocity is uniform on the transducer surface, the wave equation can be simplified to

$$\psi\left(\mathbf{r}_1, \mathbf{r}_3, t\right) == \int_T v\left(t_3\right) \int_S g\left(\mathbf{r}_1, t|\mathbf{r}_3+\mathbf{r}_4, t_3\right) d^2\mathbf{r}_4 dt_3 \tag{2.14}$$

In this equation, we can call

$$\begin{aligned} h\left(\mathbf{r}_1, \mathbf{r}_3, t-t_3\right) &= \int_S g\left(\mathbf{r}_1, t|\mathbf{r}_3+\mathbf{r}_4, t_3\right) d^2\mathbf{r}_4 \\ &= \int_S \frac{\delta\left(t-t_3-\left|\mathbf{r}_1-\mathbf{r}_3-\mathbf{r}_4\right|/c_0\right)}{2\pi\left|\mathbf{r}_1-\mathbf{r}_3-\mathbf{r}_4\right|} d^2\mathbf{r}_4 \end{aligned} \tag{2.15}$$

the spatial impulse response which is a function of spatial location and time. Therefore, we can rewrite the equation as the convolution.

$$\psi\left(\mathbf{r}_1, \mathbf{r}_3, t\right) = v(t) * h\left(\mathbf{r}_1, \mathbf{r}_3, t\right) \tag{2.16}$$

where $v(t)$ is the piston velocity waveform and h depends on the difference between r_1 and r_3. So we finally get the pressure incident field:

$$\begin{aligned} p\left(\mathbf{r}_1, \mathbf{r}_3, t\right) &= \rho_0 \frac{\partial \psi\left(\mathbf{r}_1, \mathbf{r}_3, t\right)}{\partial t} \\ &= \rho_0 v(t) * \frac{\partial h\left(\mathbf{r}_1, \mathbf{r}_3, t\right)}{\partial t} \\ &= \rho_0 \frac{\partial v(t)}{\partial t} * h\left(\mathbf{r}_1, \mathbf{r}_3, t\right) \end{aligned} \tag{2.17}$$

Therefore, the ultrasound field can be found by convolving the spatial impluse response of the transducer with the excitation function.

2.3. Calculation of the Scattered Field

After calculating the incident field pressure, we will consider the scattered field from a small inhomogeneity embedded in a homogeneous surrounding as in figure 2.2.

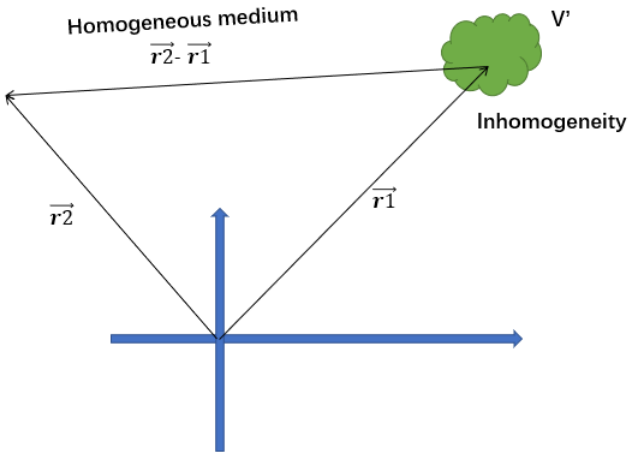

Figure 2.2. Coordinate system for calculating the scattered field.

As the figure shows, the inhomogeneity is denoted by r_1 and its volume is V'. We will calculate the scattered field at the point denoted by r_2. To do that, we need to integrate all the spherical waves emanating from the inhomogeneity V' by using the time-dependent Green's function for unbounded space. Then, the scattered field can be written:

$$\begin{aligned} p_x(\mathbf{r}_2,t) = \int_V \int_T \Bigg[& \frac{1}{\rho_0} \nabla \left[\Delta\rho(\mathbf{r}_1)\right] \cdot \nabla_{p_1}(\mathbf{r}_1,t_1) \\ & - \frac{2\Delta c(\mathbf{r}_1)}{c_0^3} \frac{\partial^2 p_1(\mathbf{r}_1,t_1)}{\partial t^2} \Bigg] \\ & \times G(\mathbf{r}_1,t_1|\mathbf{r}_2,t)\, dt_1 d^3\mathbf{r}_1 \end{aligned} \tag{2.18}$$

Where d^3r_1 means integrating with respect to r_1 over the volume V' and T means the

integration over time. The Green's function can be written as:

$$G\left(\boldsymbol{r}_1, t_1 | \mathbf{r}_2, t\right) = \frac{\delta\left(t - t_1 - \left|\mathbf{r}_2 - \mathbf{r}_1\right| / c_0\right)}{4\pi\left|\mathbf{r}_2 - \mathbf{r}_1\right|} \tag{2.19}$$

The integral can't be solved directly. We can use the Born-Neumann expansion to solve it. For simplifying the calculation, let's denote F_{op} the scattering operator.

$$F_{\mathrm{op}} = \frac{1}{\rho_0}\nabla\left[\Delta\rho\left(\mathrm{r}_1\right)\right]\cdot\nabla - \frac{2\Delta c\left(\mathrm{r}_1\right)}{c_0^3}\frac{\partial^2}{\partial t^2} \tag{2.20}$$

and G_i to be the integral operator representing Green's function. Therefore, the first-order Born approximation is :

$$p_{s_1}\left(\mathbf{r}_2, t\right) = G_i F_{\mathrm{op}} p_i\left(\mathbf{r}_1, t_1\right) \tag{2.21}$$

and then the general expression for the scattered field is:

$$\begin{aligned} p_s\left(\mathbf{r}_2, t\right) =& G_i F_{\mathrm{op}}\, p_i\left(\mathbf{r}_1, t_1\right) \\ &+ \left(G_i F_{\mathrm{op}}\right)^2 p_i\left(\mathbf{r}_1, t_1\right) \\ &+ \left(G_i F_{\mathrm{op}}\right)^3 p_i\left(\mathbf{r}_1, t_1\right) \\ &+ \left(G_i F_{\mathrm{op}}\right)^4 p_i\left(\mathbf{r}_1, t_1\right) + \cdots \end{aligned} \tag{2.22}$$

Since the scattering from small obstacles is very small, the higher-order terms can be neglected. Therefore, in practice, we only apply the first-order Born approximation. And finally equation (2.23) can be simplified as:

$$\begin{aligned} p_s\left(\mathbf{r}_2, t\right) \approx \int_{V'}\int_T \Bigg(& \frac{1}{\rho_0}\nabla\left[\Delta\rho\left(\mathbf{r}_1\right)\right]\cdot\nabla p_i\left(\mathbf{r}_1, t_1\right) \\ & - \frac{2\Delta c\left(\mathbf{r}_1\right)}{c_0^3}\frac{\partial^2 p_i\left(\mathbf{r}_1, t_1\right)}{\partial t^2}\Bigg) \\ & \times G\left(\mathbf{r}_1, t_1 | \mathbf{r}_2, t\right) dt_1 d^3\mathbf{r}_1 \end{aligned} \tag{2.23}$$

Where P_i is the incident pressure field and it can be found by convolving the spatial impluse response of the transducer with the excitation function (equation 2.17).

CHAPTER 3
PROPOSED METHODOLOGY

3.1. Proposed Method

Assume that there is an ultrasound transmitter and a receiver on the surface of a body. Meanwhile, there is also a scatterer inside the body. The transmitter sends out a short pulse δ(t) which travels through the body as a spherical spatiotemporal wave. The wave hits the scatterer and is back-scattered. Then the reflected wave is received by the receiver as shown in Fig 3.1.

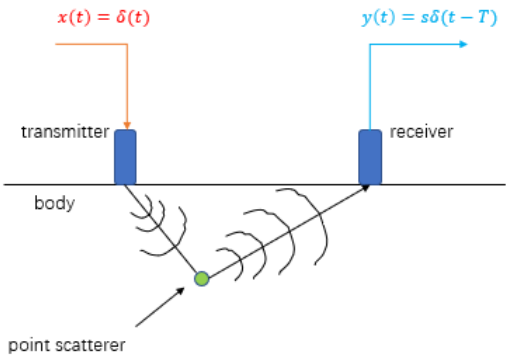

Figure 3.1. Configuration for a single scatterer.

Suppose that s is the strength of the scatterer and T is the total travel time of the transmitted wave through the body. The received signal $y(t) = s\delta(t-T)$ is the transmitted pulse delayed by T seconds and weighted by the strength of the scatterer.

Now we consider the more common situation. Let $\vec{r}_t(\theta)$ be a vector in polar coordinates

for our 2-D space that traces out an ellipse through tissue corresponding to a total travel time t from the transmitter to receiver. The transmitter and receiver are located at the foci of the ellipse and the angle θ goes from 0 to π. The lager travel time, the deeper the ellipse. Suppose there is a large continuous distribution of scatterers in the body, $s(\cdot)$, as shown in Fig 3.2.

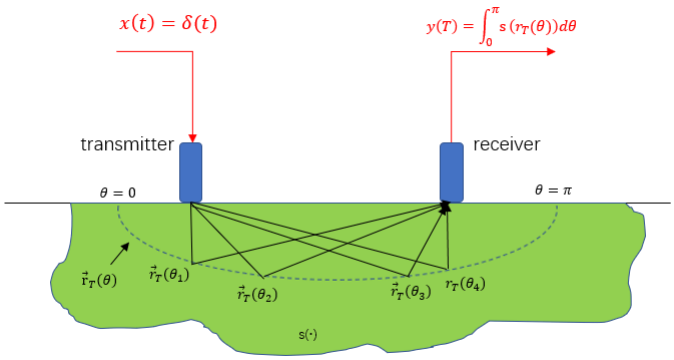

Figure 3.2. Configuration for a multiple scatterers.

The distribution is not uniform and results in uneven backscattering to the receiver. If we fix the travel time at $t = T$, each scatterer in this ellipse follows the function $s(\vec{r}_t(\theta))$. In figure 3.2, we choose four scatterers located at $\vec{r}_T(\theta_1), \vec{r}_T(\theta_2), \vec{r}_T(\theta_3)$, and $\vec{r}_T(\theta_4)$ along path $\vec{r}_T(\theta)$ respectively. Like we discussed in figure 3.1, the received signal from these four scatterers at travel time T is given by

$$y(T) = s(\vec{r}_T(\theta_1)) + s(\vec{r}_T(\theta_2)) + s(\vec{r}_T(\theta_3)) + s(\vec{r}_T(\theta_4)) \tag{3.1}$$

Therefore, the received signal from all scatterers along the path $s(\vec{r}_T(\theta))$ is

$$y(T) = \int_0^\pi s(\vec{r}_T(\theta))d\theta \tag{3.2}$$

Our goal is to estimate $s(\vec{r}_T(\theta))$ from $y(T)$. Let $p(\vec{r}_T(\theta))$ be the pressure along the ellipse

vary with θ. Then the recevied signal is given by:

$$y(T) = \int_0^{\pi} p(\vec{r}_T(\theta))s(\vec{r}_T(\theta))d\theta \tag{3.3}$$

The main idea in this method is to send out k spatiotemporal waves $p_k(\vec{r}_T(\theta))$ and gather the responses $y_k(T)$which can be expressed by

$$y_k(T) = \int_0^{\pi} p_k(\vec{r}_T(\theta))s(\vec{r}_T(\theta))d\theta, k = 1, 2, ..., N \tag{3.4}$$

which can be approximated by the sum,

$$y_k(T) = \sum_i p_k(\vec{r}_T(\theta_i))s(\vec{r}_T(\theta_i))\Delta_i, k = 1, 2, ..., N \tag{3.5}$$

Therefore, this system can be viewed as a linear system of equations:

$$As = y \tag{3.6}$$

which can be solved for the scatterer distribution $s(\cdot)$ on $\vec{r}_T(\theta_i)$. In equation (3.6), A is an N x M matrix and the ith row of the matrix represents the known samples of the transmitted wave $p_k(\vec{r}_T(\theta_i)), i = 1, ..., M$, s is an $M \times 1$ vector representing the unknown scatterers $s(\vec{r}_T(\theta_i)), i = 1, ..., M$, and y is an $N \times 1$ vector representing the received signal $y_k(T), k = 1, ..., N$.

Let $N \geq M$, which means we have more equations than unknowns. If the transmitted waves $p_k(\vec{r}_T(\theta_i))$ are known along $\vec{r}_T(\theta_i)$ and they are sufficiently independent, then the system of equations described in 3.4 can be solved to find the scattering coefficients $s(\vec{r}_T(\theta_i))$.

It should be noticed that if the transmitter and receiver are set up in the same location which means there is only one transducer on the body, the path $\vec{r}_T(\theta)$ will be a circle. Therefore all equations we discussed above also apply to this circle path case.

The solution to the least square problem is:

$$\widehat{s} = (A^T A)^{-1} A^T y \tag{3.7}$$

CHAPTER 4
EXPERIMENTAL AND RESULTS

4.1. Field II Platform Introduction

Field II is a program for the simulation of ultrasound systems. It is based on the concept of the spatial impulse response developed by Tupholme and Stepanishen and can calculate the ultrasound field for both the emitted ultrasound field and the continuous wave case. Also, all types of transducers and excitations can be simulated on it. Field II is based on MATLAB and has lots of commands for transducer simulation. Those commands are able to define transducers, set up transducer properties and calculate fields for transducers.

Our simulations in this research will be implemented on Field II. We will set up some phantoms on this platform and use our designed transducers to scan these phantoms. The pressure field matrix A and received signal y can be easily calculate by some commands on Field II. Then we are supposed to get the reflection signal s by solving the least squares problem in Chapter3.

4.2. Data Acquisition

In this section, we will discuss how we form our pressure field matrix A and received signal y in Equation (3.7).

4.2.1. Pressure Field

The ultrasound field can be found through the spatial impulse response. This response gives the emitted ultrasound field at a specific point in space as a function of time when the transducer is excitated by a dirac delta function. Then the field for any kind of excitation can by found by convolving the spatial impulse response with excitation function. There is a command to calculate the emitted field named calc_hp which will return the emitted pressure field according to the transducer and field point positions you set up.

For our case, according to our proposed methodology in Chapter 3, we set up a circular path formed by 100 field points. Each field point is a 1×3 vector (x, y, z) which represents its location. After running the command calc_hp with the field points we set up, Field II will return a 98×100 matrix. Each column indicates the change of pressure in one corresponding field point according to the wave travel time in this circle and therefore there are 100 columns in this matrix. The row number corresponds to the time length and the column number is the number of field points in this circle. The visualization of the pressure wave is :

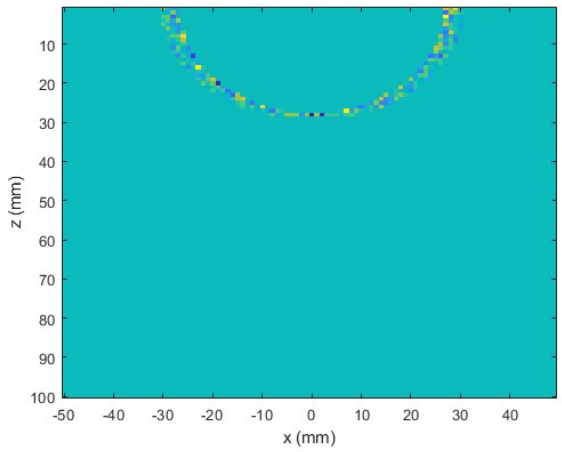

Figure 4.1. Visualization of the wave pressure.

We take the maximum value in each column because the maximum value is the pressure in this field point when the ultrasound wave is propagating on this field point. Finally, we get a 1×100 vector. Our method requires enough equations to solve the least squares problem. So, after repeating the experiment 1000 times, we will get the 1000×100 pressure matrix A.

4.2.2. Received Signal

Similar to the pressure field, there is a command named *calc_scat* which can calculate the received signal if we provide the scatterers' position and amplitude and the transmit aperture and receiver aperture. For example, the received signal for one scatterer on the circle is a 127×1 voltage trace vector, as shown in Fig.4.2.

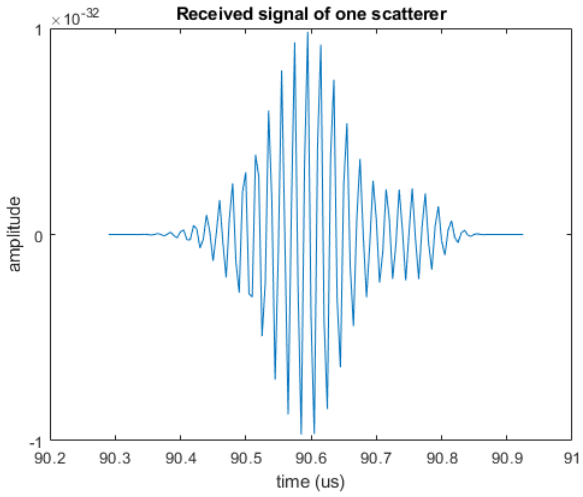

Figure 4.2. Received signal of one scattterer.

After taking the maximum value of the vector and repeating 1000 times, we get a 1000×1 received signal vector y.

4.3. Transducer Configuration

4.3.1. Transducer Parameters

In this experiment, one 128-element linear array transducer was used for both transmitting and receiving. The central frequency of the transducer was 10 MHz and the speed of sound used in this transducer was 1540 m/s which will give a wavelength of 0.154 mm. The spacing between elements was 0.0077 mm which was $\frac{1}{20}$ times the wavelength. The width of the elements was 0.000513 mm which was $\frac{1}{300}$ times wavelength. The height of each element is 0.3 mm. Also, the sampling frequency was 200 MHz.

4.3.2. Excitation Signal and Impulse Response

The basic excitation signal and impulse response of every individual elements in this method is a sequence of regularly occurring pulses, as shown in Fig.4.3. But in order to generate independent pressure patterns, the zero-mean amplitude and phase shifts are added to our basic excitation signal in every elements.

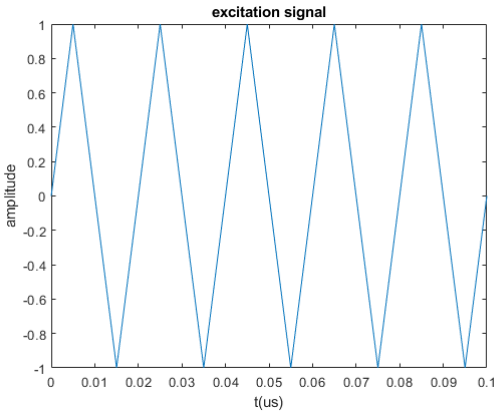

Figure 4.3. Transmitted wave.

The ultrasound pulse usually contains four or five cycles. The number of cycles can decide the length and frequency content of the pulse. The more cycles the better resolution but if the excitation is too long, there is an issue when we generate the 2-D ultrasound image as the long excitation may cover multiple cycles.

4.3.3. Generating Independent Pressure Patterns

To implement our methodology discussed in Chapter 3, we are supposed to get a full rank pressure matrix A so that we can solve the least squares problem. In other words, our transducer needs to have the ability to generate independent pressure patterns. To do so, we add zero-mean amplitude and phase shifts to our basic excitation signal. The 128 elements in our transducer are excited by 128 different waveforms so that the transducer can generate independent pressure patterns in each experiment.

The number of independent pluses transmitted will determine the noise level of the solution. If we transmit too many pluses, our solution can take a long time to calculate. To find a reasonable number of pluses, we set up two scatterers in one circle located on x=20 mm and x=30 mm respectively. We used different pulses to compare the results as shown in Fig. 4.4. After comparing, we decided to transmit 1000 pluses in all.

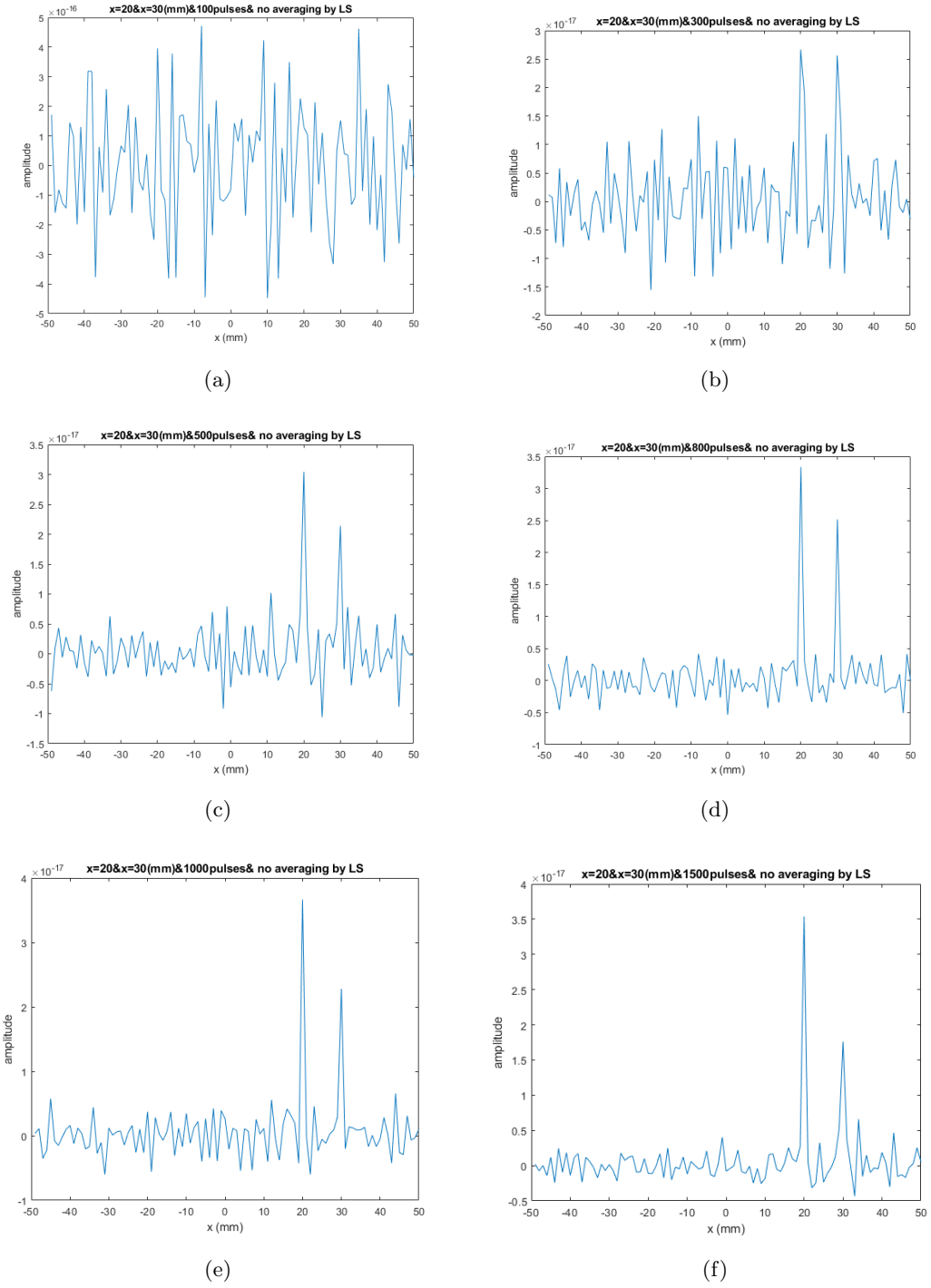

(a) (b) (c) (d) (e) (f)

Figure 4.4. Comparison in different numbers of transmitted pluses. (a) 100 pluses. (b) 300 pluses. (c) 500 pluses. (d) 800 pluses. (e) 1000 pluses. (f) 1500 pluses.

4.4. 2-D Image Formation

To build the 2-D image, we need to obtain circles at different radii which present the distance between the scatters in the circle and transducer. Different radii mean different total travel time T in the equations (3.5). By observing the received signal at different total travel time T, we can separate the interval corresponding to the circle with radii as shown in Fig 4.5. Then we use the corresponding interval to generate our received signal vector y so that we can solve the reflection signal x for this circle. A 2-D image can be generated by repeating this procedure for multiple travel times.

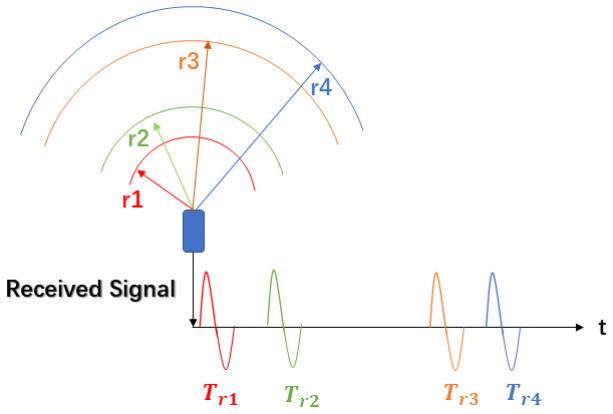

Figure 4.5. Different intervals corresponding to different radii.

In our simulation, command calc_scat in Field II returns the received voltage as a function of time. For example, Fig.4.6 represents the received signal of three scatterers at r=90mm, 100mm, and 120mm.

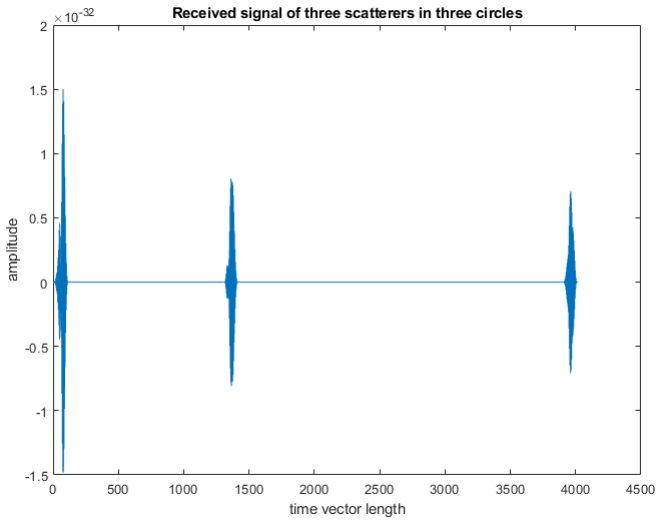

Figure 4.6. Received signal of three scatterers.

Since it starts at the first scatterer, we can calculate the start of the following scatterer time interval by :

$$n_x = fs(\frac{r_x - r_1}{1000c}) \tag{4.1}$$

where $r_1 = \frac{t_1 \times 1000c}{2}$. The length of interval in this experiment is usually 130 so that the interval we extract from the receievd signal is from n_x to n_x+135.

4.5. Results Obtained By The Proposed Method

In this section, all results in this research will be presented included 1-D and 2-D images. All our solutions calculated by least squares method were averaged by multiple times to reduce noise. We will talk about noise reduction in later section.

4.5.1. One-Dimensional Results

Our goal is to get a clear and accurate 2-D ultrasound image. To implement this, it is necessary to begin with one-dimensional scanning since it is convenient and quick for us to

adjust the transducer. At first, there is only one scatter x = 10 mm set up on the circle and after many experiments, the scanning result shows the correct location with low noise, as shown in Fig 4.7. The solution in this experiment is averaged by 10 times for reducing noise.

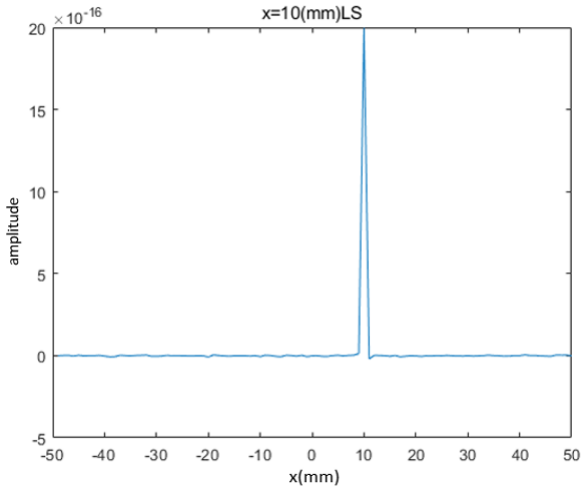

Figure 4.7. One scatterer scanned result in one-dimensional.

It is clear that the peak value at x=10mm means the scatterer is detected correctly.

For further verification of the methodology, there are more scatterers set up on the same circle. Add one scatterer after each experiment until there are six scatterers on the same circle (x=-30,-15,0,10,20,40 mm), as shown in Fig 4.8. All solutions are averaged by 10 times for reducing noise.

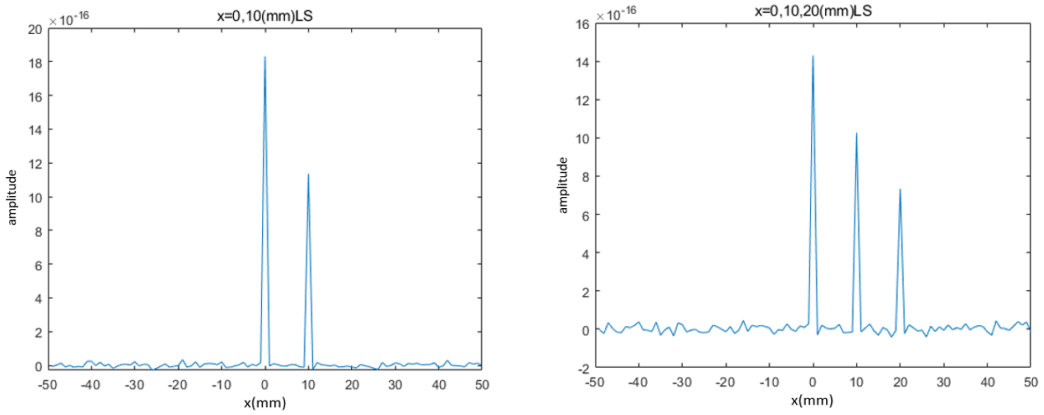

(a)

(b)

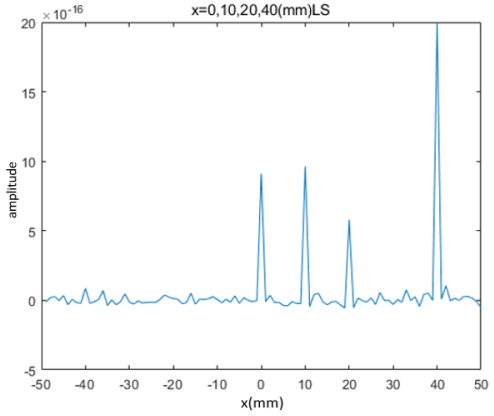

(c)

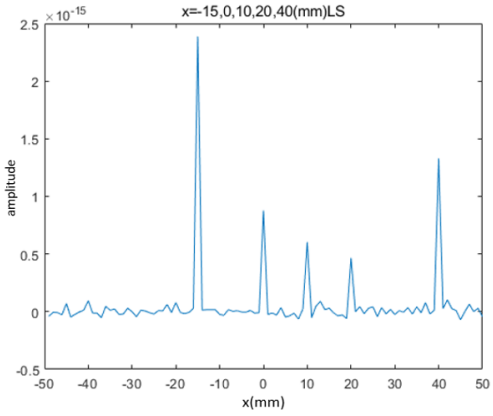

(d)

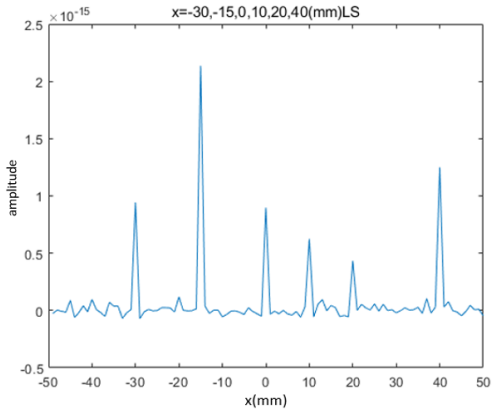

(e)

Figure 4.8. Multiple scatterers for one-dimensional case. (a) x=0,10 mm. (b) x=0,10,20 mm. (c) x=0,10,20,40 mm. (d) x=-15,0,10,20,40 mm. (e) x=-30,-15,0,10,20,40 mm.

As we can see, we can distinguish every scatterers' location clearly and correctly.

4.5.2. Two Dimensional Phantom Scanning

After detecting the location of scatterers successfully, it's time to test if this system can scan certain shape phantoms in 2-D which consisted of a triangle or square.

First, we set up a triangle phantom whose amplitude was 1 and used the same transducer to scan the phantom. The actual phantom and the image obtained by the proposed method are both shown below in fig 4.9. The solution in this experiment is averaged by 20 times for reducing noise.

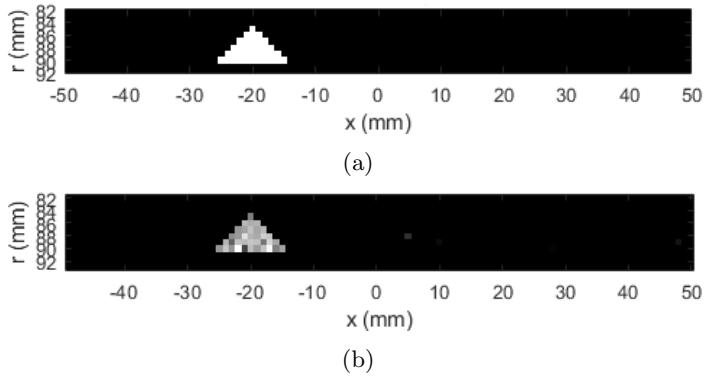

Figure 4.9. Triangle phantom. (a) Actual phantom. (b) Image obtained by the proposed method.

Then, we set up a square phantom with amplitude of 1. The actual phantom and the image obtained by the proposed method are both shown below in fig 4.10. The solution in this experiment is averaged by 20 times for reducing noise.

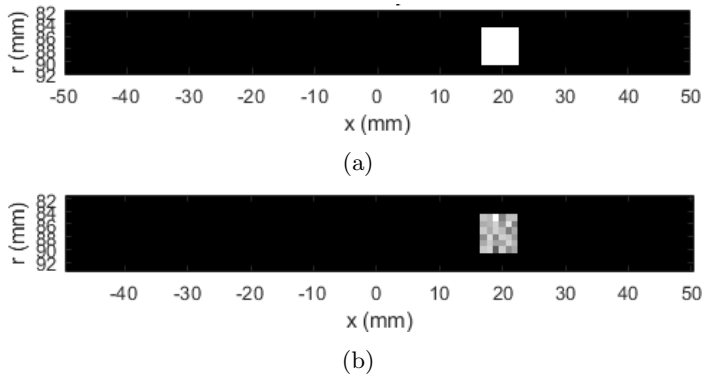

Figure 4.10. Square phantom. (a) Actual phantom. (b) Image obtained by the proposed method.

To test if the system worked with different amplitudes, we set up zero amplitude in the center of the square. The actual phantom and the image obtained by the proposed method are both shown below in Fig 4.11. The solution in this experiment is averaged by 20 times for reducing noise.

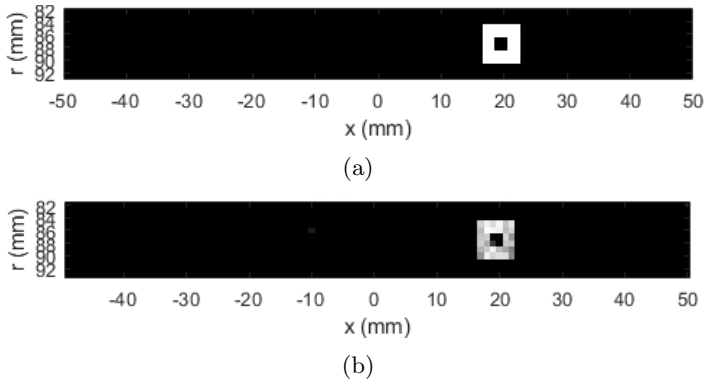

Figure 4.11. Special square phantom. (a) Actual phantom. (b) Image obtained by the proposed method.

Next, we set up two squares horizontally. The actual phantom and the image obtained by the proposed method are both shown below in Fig 4.12. The solution in this experiment

is averaged by 20 times for reducing noise.

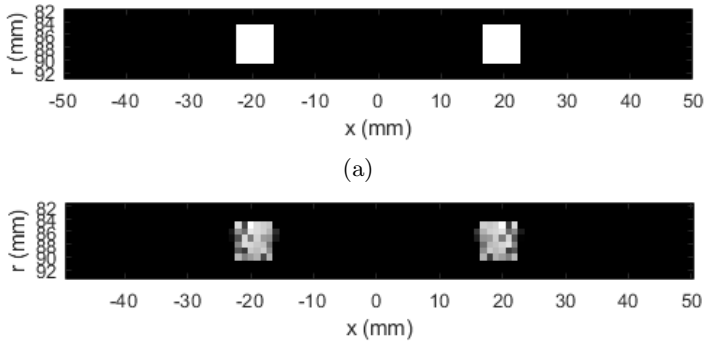

Figure 4.12. Two square phantom. (a) Actual phantom. (b) Image obtained by the proposed method.

Finally, we set up one triangle and one square horizontally. The actual phantom and the image obtained by the proposed method are both shown below in Fig 4.13. The solution in this experiment is averaged by 20 times for reducing noise.

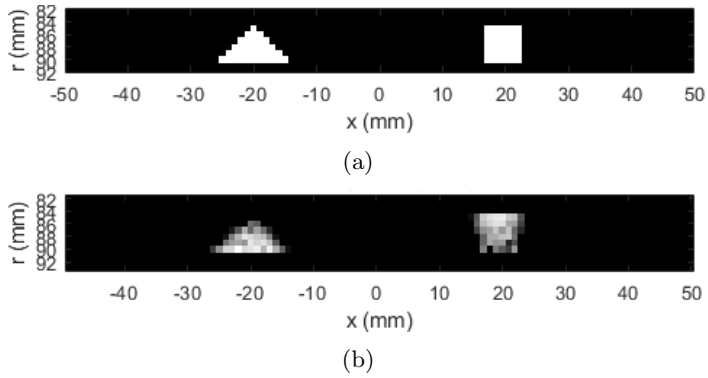

Figure 4.13. Triangle and square phantom. (a) Actual phantom. (b) Image obtained by the proposed method.

4.5.3. Artificial Kidney

If we are successful in scanning certain shape phantoms, we should able to scan human tissue. The artificial kidney is used from the Field-II website. There are other two methods to get the reflection solution from pressure field matrix A and received signal vector r which are total least square and ridge regression.

In this kidney ultrasound scanning simulation, we use these three methods to calculate the reflection signal and reconstruct the 2-D image. And the solutions from all of three method are taken the averaging of 10 times to reduce the noise. The actual artificial kidney and the image obtained by the proposed method are shown below in Fig 4.14.

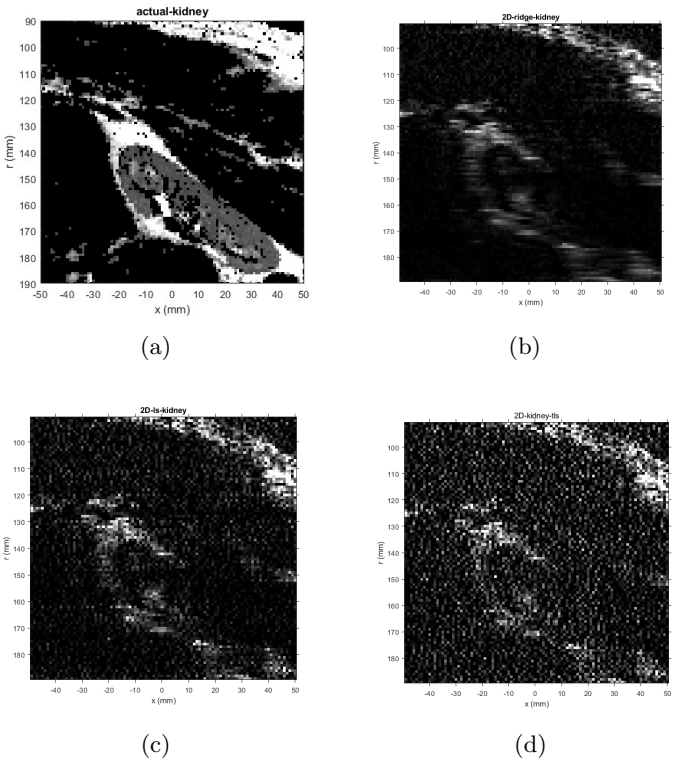

Figure 4.14. Artificial kidney simulation. (a) Actual kidney phantom. (b) Image obtained by the ridge regression method. (c) Image obtained by the least square method. (d) Image obtained by the total least square method.

As we can see, the shape of this kidney can be detected by these three methods. The ridge regression method can reduce the noise significantly but loses some resolution. The least square method and total least square have the similar appearances in this simulation.

4.6. Noise Reduction

In our method, there is some unavoidable noise what we need to deal with. To make our system linear, We average the least square solution multiple times to reduce the unwanted noise. The more times we average, the signal-to-noise ratio (SNR) will be increased which means the noise will trend to zero if we take enough averages. But we need to limit the averaging time since too many averaging time will cost a lot of time to process. In our experiment, 10-20 times averaging is enough to make the result clear and accurate. Fig 4.15 shows the comparison between no averaging and 20 times averaging in scanning the same cyst phantom.

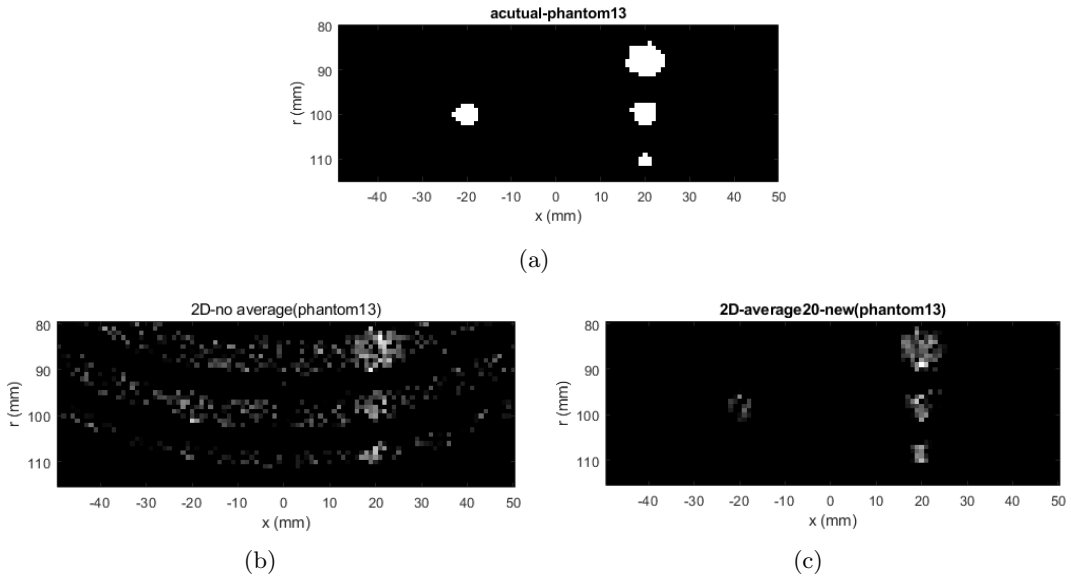

Figure 4.15. Comparison between low noise and no noise reduction. (a) actual-phantom. (b) No averaging. (c) Averaging 20 times.

As we can see there is a significant effect if we average to reduce the noise. Also, it should be noticed that our method scans the phantom circle by circle. So we need to restore our straight line result back to a circle.

CHAPTER 5
SUMMARY AND CONCLUSIONS

5.1. Summary and Conclusions

In this work we presented a method for ultrasonic imaging using random signals. The proposed approach employs random short duration pulses and unlike currently used methods, does not rely on generating narrow beams. We presented the concept of sparse transducer imaging (STI) and validated its feasibility by using the simulator Field II. It works for both on 1-D and 2-D. We scanned some artificial phantoms and got fairly accurate 2D images. The shape and size of the phantoms were restored in the image which demonstrated the feasibility of the STI concept.

Our transmit and receive transducer consists of 128 elements each of which is a separate transducer. Our goal is to design a single transducer capable of delivering variable and independent wave fronts. This may be possible by incorporating irregular surfaces on a single transducer. Field II allows for this type of design. This will be investigated in future work.

5.2. Future Work

After we generated the 2-D ultrasound image of the artificial kidney, the sparse transducer imaging (STI) concept has been proven to be effective. But there are still some challenges needed to be solved. Until now, the noise reduction in our method is based on averaging the solution, but if the target we want to scan is something moving like the heart, averaging will lead to errors.

In future work, we will continue working on reducing noise sensitivity without averaging so that we can scan live tissue. Also, we will modify our loop to significantly reduce the simulation time. After that, we plan to scan more practical medical phantoms other than the kidney. In the final step, we will design an actual transducer based on the FIELD II simulation we have done. With this transducer, we can implement the ultrasound imaging system based on our STI concept. It is worthy to further explore STI ultrasound imaging because of its potential medical value and commercial value.

BIBLIOGRAPHY

[1] Carovac, A. S. F. . J. D. "application of ultrasound in medicine. *Journal of the Society for Medical Informatics of Bosnia Herzegovina 19*, 3 (2011), 168–171.

[2] Chan, V., and Perlas, A. *Basics of Ultrasound Imaging.* 11 2011, pp. 13–19.

[3] Christensen, D. *Ultrasonic Bioinstrumentation.* WILEY, 1988.

[4] D. L. Miller, N.B.Smith, M. G. C. K., and I.Makin. Overview of therapeutic ultrasound applications and safety considerations. *Journal of Ultrasound in Medicine 31*, 4 (2012), 623–634.

[5] F. Lucchin, N. Minicuci, M. R. L. C. M. P. M. C., and Borin, P. "comparison of a-mode ultrasound and computed tomography: detection of secretion in maxillary and frontal sinuses in ventilated patients. *Intensive Care Medicine 22*, 11 (1996), 1265–1268.

[6] Halliwell, M. A tutorial on ultrasonic physics and imaging techniques. *Proceedings of Institution of Mechanical Engineers. Part H, Journal of Engineering in Medicine 224*, 2 (2000), 358–362.

[7] Jensen, J. A model for the propagation and scattering of ultrasound in tissue. *J.Acoust.Soc.Am. 89* (1991), 182–191.

[8] Jensen, J. A. *Users'guide for the Field II program.* Technical University of Denmark, 2014.

[9] Ramm, O. V., and Thurstone, F. Improved resolution in ultrasound tomography. *25th Annual Conference on Engineering in Medicine and Biology* (1972).